TRANSIENT, LARGE-SCALE 3D FINITE ELEMENT SIMULATIONS OF THE SIS100 MAGNET*

S. Koch§, T. Weiland‡, Technische Universitaet Darmstadt, D-64289 Darmstadt, Germany
H. De Gersem¶, Katholieke Universiteit Leuven - Campus Kortrijk, B-8500 Kortrijk, Belgium

Abstract

Numerical simulations are frequently used in the design, optimization and commissioning phase of accelerator components. Strict requirements on the accuracy as well as the complex structure of such devices lead to challenges regarding the numerical simulations in 3D. In order to capture all relevant details of the geometry and possibly strongly localized electromagnetic effects, large numerical models are often unavoidable. The use of parallelization strategies in combination with higher-order finite-element methods offers a possibility to account for the large numerical models while maintaining moderate simulation times as well as high accuracy. Using this approach, the magnetic properties of the SIS100 magnets designated to operate within the Facility of Antiproton and Ion Research (FAIR) at the GSI Helmholtzzentrum für Schwerionenforschung GmbH in Darmstadt, are calculated. Results for eddy-current losses under time-varying operating conditions are reported.

INTRODUCTION

For the operation of the heavy-ion synchrotron SIS100 as a part of the FAIR project at GSI, the magnetic flux density in the aperture of the dipole magnets is required to be ramped at rates as high as 4 T/s in order to keep up with the acceleration of the particles. As a consequence, eddy-current effects arising at the end regions of the dipole magnets with respect to the beam orbit, become an important issue in the magnet design and optimization process.

Despite the laminated structure of the iron yoke, eddy currents and, in turn, resistive losses appear in the conductive iron sheets. In the actual design, not only the superconductive current coils are operated at the appropriate temperature of 4.5 K, but also the the ferromagnetic yoke and the mechanical support. As a consequence, the eddy-current losses induced by fast ramping appear in the cold mass of the system. These losses increase the load of the cryogenic system and therefore the power consumption of the facility significantly. Hence, one of the design goals is to reduce the Joule losses inside the magnet to an acceptable level. Several design optimizations aimed at this issue have already been proposed, e.g. in [1], [2], whereas the Nuclotron magnet [3], [4] served as a starting point for the design. These optimizations are based on experiments as well as numerical simulations in 2D and 3D.

* Work supported by GSI Helmholtzzentrum für Schwerionenforschung GmbH, Darmstadt under contract F&E, DA-WEI1

§ koch@temf.tu-darmstadt.de
‡ thomas.weiland@temf.tu-darmstadt.de
¶ Herbert.DeGersem@kuleuven-kortrijk.be

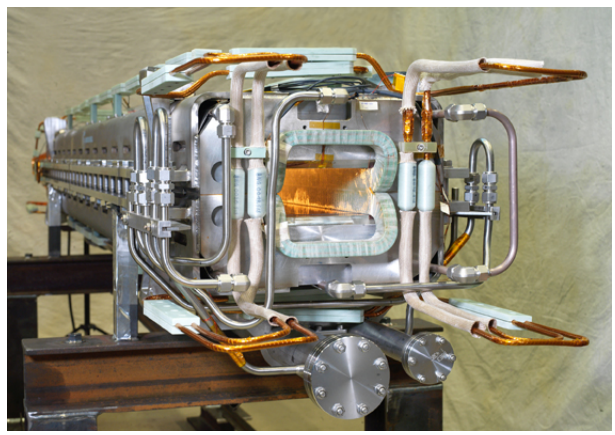

Figure 1: Full-length prototype dipole magnet for the SIS100 including cooling tubes and mechanical assembly (photograph: J. Guse, GSI (www.gsi.de)).

While the original Nuclotron magnet is 1.4 m long [4], the length of the current prototype of the SIS100 dipole shown in Fig. 1 is increased to 2.8 m [5]. Therefore, the number of dipole magnets required to cover the circumference of the synchotron is, in turn, lowered by a factor close to two when compared to a virtual installation of the short magnet. As the major fraction of the eddy currents arises at the end regions of the iron yoke, the resulting overall losses are reduced accordingly. The increased length, however, provides additional challenges regarding numerical simulations when using volume-based discretization methods such as the finite element (FE) method. It leads to larger numerical models which in turn require a longer simulation time and more computational resources. One way to deal with the large numerical models is the use of parallelization techniques. Simulations related to the full length prototype shown in Fig. 1 are carried out using the finite element method in combination with higher-order shape functions. The eddy-current losses in the different parts of the yoke assembly are calculated.

NUMERICAL MODELING

Transient Magnetoquasistatic Formulation

Even though the desired ramping of the aperture field is fast when considering the amount of energy dissipated in the electrically conductive iron yoke, the time variation of

the resulting fields still justifies the application of the magnetoquasistatic approximation the Maxwell equations. Different formulations based on potentials or field quantities can be derived as reviewed, e.g., in [6], [7]. Among these, the formulation in terms of the magnetic vector potential $\vec{A}$ is well suited for the problem under consideration. It is introduced in order to represent the magnetic flux density $\vec{B}$ according to

$$\vec{B} = \nabla \times \vec{A} \,. \tag{1}$$

This leads to the second order partial differential equation

$$\nabla \times \left(\nu \nabla \times \vec{A} \right) + \sigma \frac{\partial}{\partial t} \vec{A} = \vec{J}_\mathrm{s} \,, \tag{2}$$

where $\nu = 1/\mu$ denotes the reluctivity, μ the permeability, σ the electric conductivity and $\vec{J}_\mathrm{s}$ the source current density. Note that $\vec{A}$ is interpreted as the modified magnetic vector potential and therefore features an implicit gauge in the conductive regions [8]. The quanties of interest within this application, the electric field strength $\vec{E}$ and the magnetic flux density $\vec{B}$, are conveniently obtained from the solution for $\vec{A}$ along with its temporal derivative by

$$\vec{E} = -\frac{\partial \vec{A}}{\partial t} \tag{3}$$

and Eq. 1. In contrast to the very similar formulation in terms of the $\vec{E}$ itself, the source current density $\vec{J}_\mathrm{s}$ in Eq. 2 is not required to be differentiated in time. This is especially important as non-smooth excitation functions are provided for this type of magnet simulations.

Spatial Discretization

In order to solve the formulation in Eq. 2 numerically, tetrahedral meshing is applied. The computational domain is limited to the dipole magnet and the considered parts of the mechanical assembly. At a sufficient distance to the structure, closed boundary conditions are applied. By using vectorial FE shape functions $\vec{w}_j$ ensuring tangential continuity of the approximated quantity, the magnetic vector potential is approximated in terms of the local Ritz approach

$$\vec{A} \approx \sum_j a_j \vec{w}_j \,. \tag{4}$$

In case of a lowest order approximation six vectorial shape functions, each of which associated with one edge of a tetrahedron, are used to represent the magnetic vector potential $\vec{A}$. This approximation is capable of modeling a linear variation of the vectorial quantity $\vec{A}$ itself as well as a constant flux density $\vec{B}$ resulting from the application of the curl operator according to Eq. 1 consistently. The subsequent higher order set of shape functions, being quadratically exact in $\vec{A}$ and linearly exact in the curl of $\vec{A}$ features 20 shape functions per element and, in turn, the same number of degrees of freedom a_j in Eq. 4. Choosing the same set of shape functions as test functions $\vec{w}_i$ as part of the standard Galerkin procedure turns Eq. 2 into the weak formulation. Discretization of the latter by means of the shape functions $\vec{w}_j$ results in the semi-discrete representation of Eq. 2:

$$\mathbf{K}_\nu \mathbf{a} + \mathbf{D}_\sigma \frac{\mathrm{d}}{\mathrm{d}t} \mathbf{a} = \mathbf{j}_\mathrm{s} \,. \tag{5}$$

In this differential-algebraic equation, $\mathbf{K}_\nu$ denotes the stiffness matrix, $\mathbf{D}_\sigma$ the damping matrix, $\mathbf{a}$ collects the degrees of freedom a_j for the magnetic vector potential and the elements of $\mathbf{j}_\mathrm{s}$ describe the excitation current density weighted by the test functions $\vec{w}_i$. The entries of the matrices and vectors mentioned are given by

$$\left(\mathbf{K}_\nu\right)_{i,j} = \int_\Omega \left(\nabla \times \vec{w}_j\right) \cdot \nu \cdot \left(\nabla \times \vec{w}_i\right) \mathrm{d}V \,, \tag{6}$$

$$\left(\mathbf{D}_\sigma\right)_{i,j} = \int_\Omega \vec{w}_j \cdot \sigma \cdot \vec{w}_i \mathrm{d}V \,, \tag{7}$$

$$\left(\mathbf{j}_\mathrm{s}\right)_i = \int_\Omega \vec{J}_\mathrm{s} \cdot \vec{w}_i \mathrm{d}V \,, \tag{8}$$

where Ω denotes the computational domain and the characteristic material coefficients ν and σ are assumed to be tensor-valued.

Temporal Discretization and Linearization

The differential-algebraic representation of the magnetoquasistatic formulation in terms of the magnetic vector potential in Eq. 5 is discretized in time using the implicit Euler scheme. For constant time steps Δt indexed by n, with $t_n = t_0 + n\Delta t$, the algebraic nonlinear system of equations reads

$$\mathbf{K}_\nu \mathbf{a}^{(n+1)} + \frac{1}{\Delta t} \mathbf{D}_\sigma \mathbf{a}^{(n+1)} = \underbrace{\frac{1}{\Delta t} \mathbf{D}_\sigma \mathbf{a}^{(n)} + \mathbf{j}_\mathrm{s}^{(n+1)}}_{\mathbf{f}^{(n+1)}} \,, \tag{9}$$

whereas $\mathbf{a}^{(n+1)} = \mathbf{a}(t_{n+1})$, $\mathbf{a}^{(n)} = \mathbf{a}(t_n)$ and $\mathbf{j}_\mathrm{s}^{(n+1)} = \mathbf{j}_\mathrm{s}(t_{n+1})$. The fix-point formulation of Eq. 9 is given by $\mathbf{F}(\mathbf{a}^{(n+1)}) = 0$ with

$$\mathbf{F}(\mathbf{a}^{(n+1)}) = \mathbf{K}_\nu \mathbf{a}^{(n+1)} + \frac{1}{\Delta t} \mathbf{D}_\sigma \mathbf{a}^{(n+1)} - \mathbf{f}^{(n+1)} \,. \tag{10}$$

It is nonlinear with respect to the entries of $\mathbf{K}_\nu$ due to ferromagnetic saturation. In order to advance from the time instance t_n to t_{n+1} the nonlinear system needs to be solved. Based on Eq. 10 linearization is carried out by means of a Newton-Krylov method. The search direction $\mathbf{d}^{(n+1,k+1)}$ within each nonlinear step k is found by solving the system

$$\mathbf{J}_\mathbf{F}^{(n+1,k)} \mathbf{d}^{(n+1,k+1)} = -\mathbf{F}(\mathbf{a}^{(n)}) \tag{11}$$

with the Jacobian $\mathbf{J}_\mathbf{F}$ of $\mathbf{F}$ using a Krylov-subspace iteration. Here, the Jacobian is given in matrix form by

$$\mathbf{J}_\mathbf{F}^{(n+1,k)} = \mathbf{K}_{\nu_\mathrm{d}}^{(n+1,k)} + \frac{1}{\Delta t} \mathbf{D}_\sigma \tag{12}$$

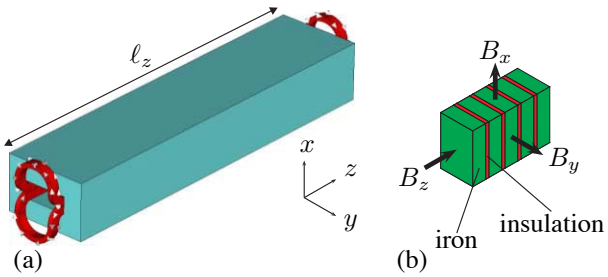

Figure 2: (a) Simplified model of the SIS100 magnet yoke and the coil; (b) Strongly enlarged view of the laminated structure of the yoke based on iron plates and insulation sheets (relation of thickness is not to scale).

while the entries of the matrix $\mathbf{K}_{\nu_\mathrm{d}}$ follow from replacing ν in Eq. 6 by the differential reluctivity tensor ν_d, as described, e.g., in [9]. As a consequence, the sparsity pattern of the Jacobian $\mathbf{J_F}$ is identical to the one of a standard system matrix in linear magnetoquasistatic modeling. From the search direction the new nonlinear iterate $\mathbf{a}^{(n+1,k+1)}$ is obtained by

$$\mathbf{a}^{(n+1,k+1)} = \mathbf{a}^{(n+1,k)} + \alpha \mathbf{d}^{(n+1,k+1)} \tag{13}$$

with the relaxation factor $\alpha = 1$ corresponding to full Newton step. A solution candidate $\mathbf{a}^{(n+1,k+1)}$ for $\mathbf{a}^{(n+1)}$ is accepted, if the criterion

$$r_\mathrm{nlin} = \frac{\left\|\mathbf{F}(\mathbf{a}^{(n+1,k+1)})\right\|_2}{\left\|\mathbf{f}^{(n+1)}\right\|_2} < \epsilon_\mathrm{nlin} \tag{14}$$

in terms of the relative nonlinear residual r_nlin is met for a prescribed tolerance ϵ_nlin. Within each nonlinear step $k+1$ the system in Eq. 11 is solved using Krylov-subspace iterations. These iterations are terminated once the appropriate residual tolerance ϵ_{k+1} for the current nonlinear step $k+1$ is reached. Using an adjustable stopping criterion ϵ_{k+1} as described in [10] can significantly reduce the total number of Krylov iterations per time step. An implementation according to [11] based on the NOX package of the TRILINOS framework [12] is used for the numerical simulations reported in this paper.

Homogenization of the Laminated Yoke Material

A schematic view of the SIS100 dipole reduced to the ferromagnetic yoke and the current coil is shown in Fig. 2(a). Due to the high ramp rate required for the application in the synchrotron, the yoke is built from laminated steel plates as indicated in Fig. 2(b). It is, however, cumbersome if not impossible to resolve the very thin insulation layers between adjacent iron sheet within a 3D numerical simulation. Therefore, the packing factor γ_p, commonly employed to classify laminated steels, is used to construct a homogeneous, anisotropic material to be considered in the simulation. For a straight yoke the co-ordinates can be aligned with the main axes of the anisotropy. As a consequence, diagonal tensors

$$\nu = \mathrm{diag}\left(\nu_{xx}, \nu_{yy}, \nu_{zz}\right); \; \sigma = \mathrm{diag}\left(\sigma_{xx}, \sigma_{yy}, \sigma_{zz}\right) \tag{15}$$

for the reluctivity ν and the conductivity σ are sufficient to model the homogenized yoke material as described in [13].

While in general (case A) all entries of the reluctivity tensor in Eq. 15 are dependent on the value of the magnetic flux density as well as on the packing factor γ_p, a simplification can be introduced at moderate saturation levels up to 1.6 T [14]. Namely, the reluctivity ν_{zz} is observed to be constant with respect to the saturation level and it is only related to the packing factor by $\nu_{zz} = \nu_0(1-\gamma_\mathrm{p})$. This type of modeling the anisotropic yoke material is referred to as case B in the following. Details and a comparison of both material models with respect to the eddy-current losses in the yoke can be found in [13].

BENCHMARK MODEL

The results reported in the following sections are obtained by using an in-house simulation tool based on the FEMSTER library [15] for the FE layer and the TRILINOS framework [12] for the linear algebra infrastructure as well as parallelized matrix and vector classes in terms of MPI [16]. Pre- and postprocessing as well as automatic mesh generation is carried out in CST STUDIO SUITE™ [17].

Simulation Setup

In order to validate the simulation tool in terms of a comparison of the results for the eddy-current losses to the ones obtained by other codes, a simplified benchmark model of the SIS100 dipole was defined [14], [18]. The according geometry is shown in Fig. 2(a). Further parameters for the magnetoquasistatic simulations of the simplified model can be summarized as follows:

- Length of the iron yoke $\ell_z = 1200$ mm;
- Outer dimensions of the rectangular cross-section of the yoke: 276 mm × 186 mm;
- Aperture size 146 mm × 56.4 mm;
- Conductivity tensor of the laminated steel: $\sigma_{xx} = \sigma_{yy} = 3.2 \cdot 10^6$ S/m, $\sigma_{zz} = 0$;
- Maximum excitation current: $I_\mathrm{max} = 48$ kA;
- Coil excitation: triangular cycle $0 \ldots 48$ kA$\ldots 0$ of 1 s duration ($\partial B/\partial t = 4$ T/s);
- Homogeneous, anisotropic, nonlinear yoke material for different values of the packing factor γ_p (case A, case B);
- Constant time step $\Delta t = 0.01$ s.

Convergence of the Eddy-Current Losses

On the basis of the discretized model several simulations are carried out. In a first set, the eddy-current losses are calculated for different values of the packing factor γ_p in the range of 0.93 to 0.98. The losses are evaluated in each

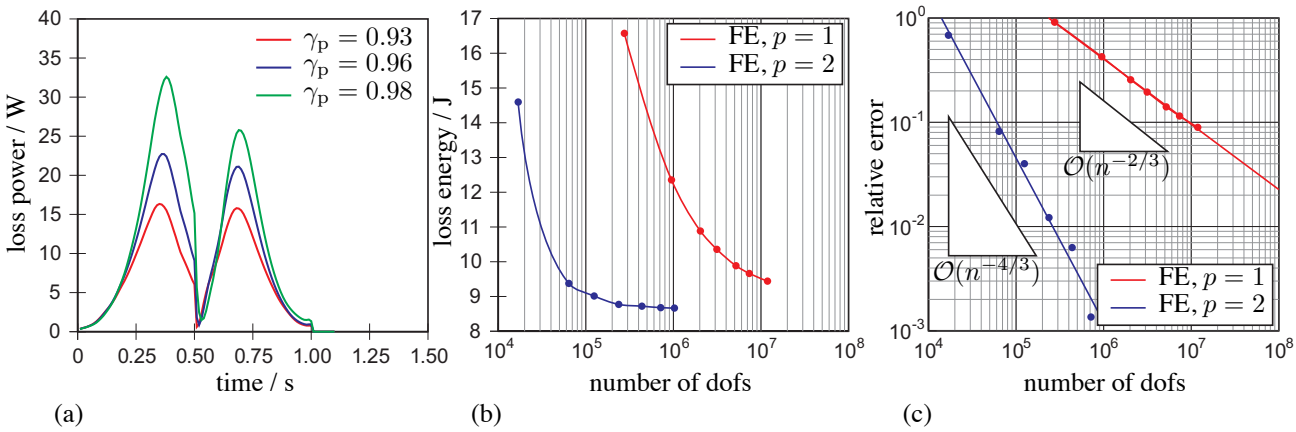

Figure 3: (a) Time dependence of the volume-integrated eddy-current losses in the magnet yoke in a triangular excitation cycle for different values of the packing factor γ_p. (b) Convergence of the loss energy integrated over the length of the excitation cycle for different levels of discretization: For lowest order shape functions ($p = 1$) and for shape functions allowing for a linear variation ($p = 2$) of the curl of the primary unknown. (c) Convergence of the relative discretization error of the power losses with respect to a reference solution obtained using 10^6 degrees of freedom (dofs) in combination with linear shape functions ($p = 2$).

time step and integrated spatially over the entire yoke volume. Fig. 3(a) shows the results on the time-axis. While the curves agree at the beginning of the cycle, the losses increase differently due to beginning ferromagnetic saturation starting approximately at $t = 0.2$ s. For higher packing factors the resulting eddy-current losses become larger. However, a high value is required in order to avoid adversely affecting the magnetic length of the dipole.

A second set of simulations addresses the discretization error of the numerical simulation which is quantified in terms of the loss energy over one excitation cycle, here. In order to compare the results to the ones reported in [18], the simplified homogenization strategy (case B) is implemented in the simulation tool. Using automatic mesh generation, several discrete representations of the magnet model are created. These are equipped with either lowest ($p = 1$) or second order ($p = 2$) FE shape functions. For each selected combination of a FE mesh and one of the sets of shape functions, a transient nonlinear simulation is carried out. The results of the integrated, time-averaged losses are shown in Fig. 3(b) with respect to the according number of degrees of freedom (dofs). Very large numerical models are required in order to obtain reliable results from the simulation, in particular for the case of lowest order shape functions. This becomes even more evident when determining the relative error which is illustrated in Fig. 3(c). Here, a simulation involving approximately 10^6 dofs based on second order FE shape functions provides the reference solution for the eddy-current losses. The higher approximation order of the linear shape functions leads to an improved convergence in terms of the discretization error. As a consequence, a fixed accuracy can be achieved using fewer degrees of freedom when compared to the curve related to the lowest order shape functions. Furthermore, the high accuracy required for the application can only be reached using the higher order shape functions as, e.g., a discretization involving ten million lowest order degrees of freedom only achieves an accuracy of around 1%. The slope of the curves agrees with the theoretically expected values for the respective order of approximation.

Comparison to Different Simulation Code

Using the simplified homogenization model (case B) for the laminated iron yoke, the results for the eddy-current losses can directly be compared to results from the literature. The first two results columns of Table 1 show the time-integrated losses in the magnet yoke for the two different material models obtained by using the in-house simulation tool. For comparison, the third column contains the values reported in [14], [18]. The difference in the results for the two material models increases for higher packing factors and reaches up to 20% for $\gamma_p = 0.98$. However, when comparing the last two columns of Table 1 for case B, a good agreement within 2.5% is observed for lower packing factors. The remaining differences can be assigned to the boundary conditions, which were not exactly specified in advance. Further contributions might be found in the temporal discretization as well as in the coil modeling.

Table 1: Time-integrated eddy-current losses for different values of the packing factor γ_p using a nonlinear (case A) as well as a constant reluctivity (case B) in z-direction.

packing factor γ_p	**case A** Fig. 3(a)	**case B** Fig. 3(b)	**case B** cf. [14], [18]
0.93	7.68 J	8.77 J	8.66 J
0.96	9.86 J	11.58 J	11.30 J
0.98	12.51 J	15.05 J	13.90 J

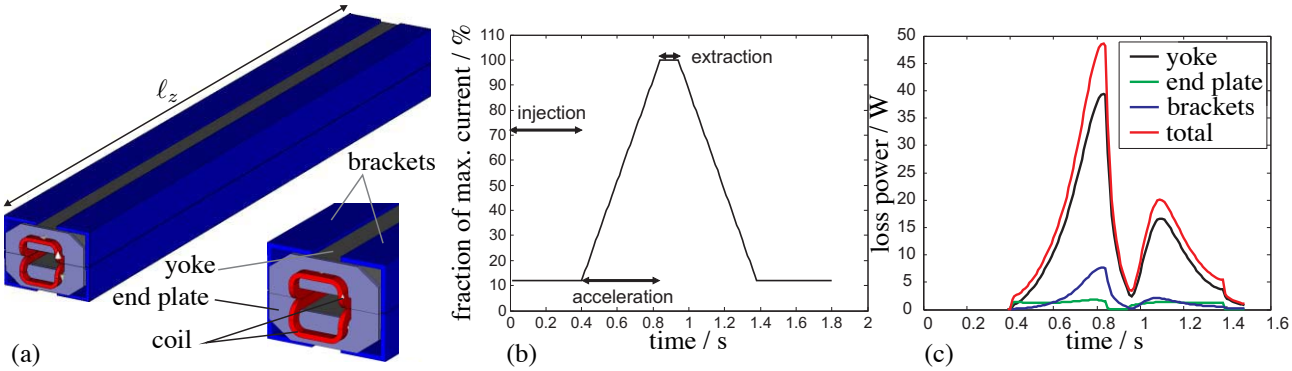

Figure 4: (a) CAD model of the full-length SIS100 dipole ($\ell_z = 2.8$ m) containing yoke, end plates and brackets ensuring mechanical stability. The new model uses a modified, lower coil design in order to reduce the eddy-current losses in the end regions. (b) Realistic excitation cycle resulting in a maximum aperture field of 2.1 T. (c) Eddy-current losses with respect to time for the separate parts of the yoke assembly.

SIMULATION RESULTS FOR THE FULL-LENGTH DIPOLE MAGNET

Using the in-house simulation software described above, a new set of simulations is carried out on the basis of more realistic parameters for the yoke geometry and for the excitation signal. A design featuring a long yoke offers advantages regarding the magnitude of the eddy-current losses as well as the homogeneity of the magnetic flux density in the aperture region. The geometry used for the simulations reported in the following is outlined in Fig. 4(a). End plates and brackets made from stainless steel, included for mechanical stability, are considered in the simulations as these parts are supposed to contribute to the overall losses in the magnet. In contrast to prior simulations, a more realistic operation cycle, as shown in Fig. 4(b), is considered. Further parameters, as far as differing from the previous setup, are as follows:

- Length of the iron yoke $\ell_z = 2800$ mm;
- Thickness of endplates and brackets; $d = 15$ mm;
- Isotropic conductivity of stainless steel used for end plates and brackets: $\sigma_{\mathrm{steel}} = 2.0 \cdot 10^6$ S/m;
- Isotropic permeability of stainless steel: $\mu_{\mathrm{steel,r}} = 1.01$;
- Coil excitation: as indicated in Fig. 4(b);
- Homogeneous, anisotropic, nonlinear yoke material, packing factor $\gamma_{\mathrm{p}} = 0.98$ (case A).

Due to the increased length of the magnet yoke, a larger number of tetrahedra is required for the numerical model when compared to the benchmark model. The superior convergence of higher-order shape functions ($p = 2$) is exploited in order to achieve the desired accuracy in an acceptable time. As the parallelization of the simulation tool is implemented on the basis of MPI, shared-memory as well as distributed-memory computing environments can be used. The results for the eddy-current losses shown in Fig. 4(c) are obtained on a workstation featuring two quad-core processors. A typical transient nonlinear simulation of this type takes approximately 36 hours, the major part of which is spent on the solution of the linear systems of equations. In Fig. 4(c) the time-characteristic of the eddy-current losses in the different parts of the yoke assembly are illustrated. The losses in the ferromagnetic yoke form the major contribution to the overall losses in this setup. Due to the high packing factor and the resulting anisotropic properties, relaxation effects arise and in turn lead to different magnitudes of the two maxima [19]. Also for the brackets, relaxation effects typical for the isotropic case equivalent to a packing factor $\gamma_{\mathrm{p,steel}} = 1$ are observed in terms of an almost vanishing second maximum in the loss characteristic. As the end plates are thin and feature a smaller electrical conductivity as the laminated steel, the magnitude of the resulting losses is very small when compared to the remaining contributions. Furthermore, the respective relaxation time is short with respect to the considered simulation interval. Therefore, the loss characteristic is similar to the one expected for an equivalent linear RL-network related to the respective part of the model. Table 2 shows the integrated losses over the excitation cycle depicted in Fig. 4(b) for two different discretizations. The second column corresponds to the results of Fig. 4(c). In Fig. 5 the magnitude of the z-component of the magnetic flux density, which is responsible for the eddy currents, is shown in the end-region of the magnet. The sub-figures correspond to time-instances at the beginning (Fig. 5(a)), in the middle (Fig. 5(b)) and at the end of the acceleration phase.

Table 2: Eddy-current losses in the separate parts of the yoke assembly for two different levels of discretization both using FE shape functions of second order ($p = 2$).

Discretization	433 246 **dofs**	791 072 **dofs**
yoke	12.97 J	12.73 J
end plates	1.19 J	1.18 J
bracket	1.95 J	1.95 J
total	16.11 J	15.85 J

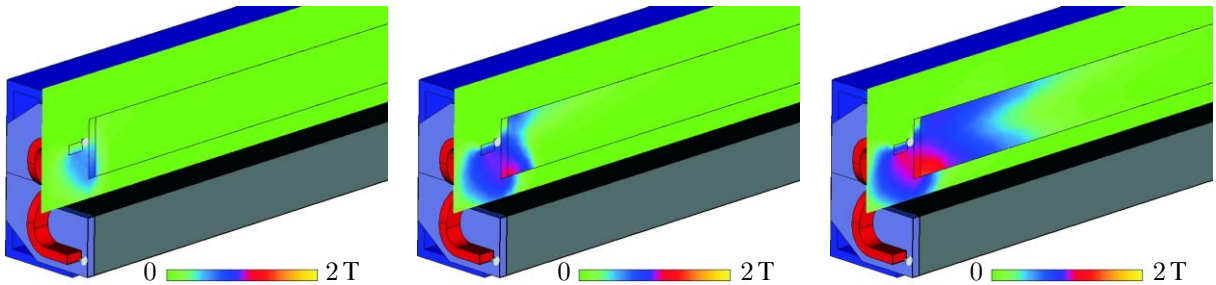

(a) (b) (c)

Figure 5: Magnitude of the z-component of the magnetic flux density responsible for the eddy-currents at the end regions of the yoke assmbly in logarithmic color scale at different time instances: (a) $t = 0.42$ s, (b) $t = 0.68$ s, (c) $t = 0.82$ s.

CONCLUSION

Transient, nonlinear simulations required to predict the eddy-current losses in the SIS100 dipole are carried out by means of a 3D finite element simulation tool. The results are compared to a different, independent simulation code on the basis of a benchmark model. A good agreement in terms of the calculated eddy-current losses is observed. The developed simulation tool is well suited for the simulation of large and geometrically complicated structures. Thanks to the parallelized simulation framework, it is further scalable to even larger numerical models while maintaining moderate computational times as well as high accuracy by using higher-order finite element shape functions.

REFERENCES

[1] A. Kalimov, E. Fischer, G. Hess, G. Moritz, and C. Mühle. Investigation of the power losses in a laminated dipole magnet with superconductive coils. *IEEE Trans. Appl. Supercond.*, 14(2):267–270, June 2004.

[2] A. Kovalenko, N. Agapov, E. Fischer, H. Khodzhibagiyan, G. Kuznetsov, G. Moritz, and A. Smirnov. New results on minimizing ac power losses in a fast cycling 2 T superferric dipole with a cold yoke. *IEEE Trans. Appl. Supercond.*, 16(2):338–341, June 2006.

[3] A.M. Baldin, N.N. Agapov, S.A. Averichev, A.M. Donyagin, E.I. D'yachkov, H.G. Khodzhibagiyan, A.D. Ko valen ko, L.G. Makarov, E.A. Matyushevsky, and A.A. Smirnov. Superconducting fast cycling magnet of the Nuclotron. *IEEE Trans. Appl. Supercond.*, 5(2):875–877, June 1995.

[4] A. Kovalenko. Status of the Nuclotron. In *Proceedings of the 4th European Particle Accelerator Conference (EPAC94)*, pages 161–164, London, UK, June 1994.

[5] E. Fischer, H.G. Khodzhibagiyan, and A.D. Kovalenko. Full size model magnets for the fair sis100 synchrotron. *IEEE Trans. Appl. Supercond.*, 18(2):260–263, June 2008.

[6] O. Bíró and K. Preis. On the use of the magnetic vector potential in the finite element analysis of three-dimensional eddy currents. *IEEE Trans. Magn.*, 25(4):3145–3159, July 1989.

[7] O. Bíró and K. Preis. Finite Element Analysis of 3-D Eddy Currents. *IEEE Trans. Magn.*, 26(2):418–423, March 1990.

[8] C.R.I. Emson and J. Simkin. An Optimal Method for 3-D Eddy Currents. *IEEE Trans. Magn.*, MAG-19(6):2450–2452, November 1983.

[9] S. Koch, H. De Gersem, and T. Weiland. Transient 3D finite element simulations of the field quality in the aperture of the SIS-100 dipole magnet. *IEEE Trans. Appl. Supercond.*, 19(3):1162–1166, June 2009.

[10] R.S. Dembo, S.C. Eisenstat, and T. Steihaug. Inexact Newton methods. *SIAM J. Numer. Anal.*, 19(2):400–408, April 1982.

[11] M. Pernice and H.F. Walker. NITSOL: A Newton iterative solver for nonlinear systems. *SIAM J. Sci. Comput.*, 19(1):302–318, January 1998.

[12] M. Heroux, R. Bartlett, V. Howle, R. Hoekstra, J. Hu, T. Kolda, R. Lehoucq, K. Long, R. Pawlowski, E. Phipps, A. Salinger, H. Thornquist, R. Tuminaro, J. Willenbring, and A. Williams. An overview of Trilinos. *Sandia National Laboratories, SAND2003-2927*, 2003.

[13] S. Koch, H. De Gersem, T. Weiland, E. Fischer, and G. Moritz. Transient 3D finite element simulations of the SIS100 magnet considering anisotropic, nonlinear material models for the ferromagnetic yoke. *IEEE Trans. Appl. Supercond.*, 18(2):1601–1604, June 2008.

[14] E. Fischer, R. Kurnyshov, G. Moritz, and P. Shcherbakov. 3-D transient process calculations for fast cycling superferric accelerator magnets. *IEEE Trans. Appl. Supercond.*, 16(2):407–410, June 2006.

[15] D. White, P. Castillo, B. Fasenfest, R. Rieben, and M. Stowell. FEMSTER: A C++ class library of higher-order discrete differential forms. *Lawrence Livermore National Laboratory*, 2006.

[16] MPI. Argonne National Laboratory, Argonne, IL, USA. www.mcs.anl.gov.

[17] CST STUDIO SUITE™. Computer Simulation Technology AG, Darmstadt, Germany. www.cst.com.

[18] P. Shcherbakov, E. Fischer, and R. Kurnyshov. 3D magnetic field and eddy loss calculations for iron dominated accelerator magnets using ansys compared with results of non-commercial codes. In *Proceedings of the EPAC 2006*, pages 2595–2597, Edinburgh, Scotland, UK, 2006.

[19] E. Fischer, R. Kurnyshov, and P. Shcherbakov. Analysis of the eddy current relaxation time effects in the FAIR SIS 100 main magnets. *IEEE Trans. Appl. Supercond.*, 17(2):1173–1176, June 2007.